THE JOURNAL OF PHYSICAL CHEMISTRY C
A JOURNAL OF THE AMERICAN CHEMICAL SOCIETY

pubs.acs.org/JPCC

Article

Toward the Mechanism of *o*-Xylene Isomerization in Selected Zeolites of Different Si/Al Ratios and Channel Sizes—Experiment Corroborated by Periodic DFT + D Simulations

Gabriela Jajko, Karolina Tarach, Kinga Góra-Marek, Paweł Kozyra, and Witold Piskorz*

Cite This: *J. Phys. Chem. C* 2021, 125, 10334−10348

Read Online

ACCESS | Metrics & More | Article Recommendations

ABSTRACT: The present work comprises the characterization of zeolite properties in the view of their usability as catalysts in the isomerization of xylenes and ethanol-to-hydrocarbon (ETH) process. Therefore, the intermediate products of these reactions have been proposed as the 5- and 7-membered hydrocarbon ring structures. The quantum chemical calculations were carried out at the periodic DFT GGA + D level of theory to optimize the structures of zeolites and xylenes and the protonated forms of the latter. The isomerization and the ETH processes have similar intermediate products; their identification is not, however, possible spectroscopically; hence, the quantum chemical calculations deemed necessary. The calculations include thermal effects—the entropic contributions were calculated via the classic, harmonic vibrational analysis, and the Gibbs free energies were calculated at T = 298 K, the temperature at which the spectra of gaseous and adsorbed species were recorded. Based on the analysis of the contributions to the adsorption energy of the hydrocarbon 5- and 7-membered ring structures and having verified the results via comparison of the calculated IR spectra to the experimental ones, the most probable intermediate products were proposed.

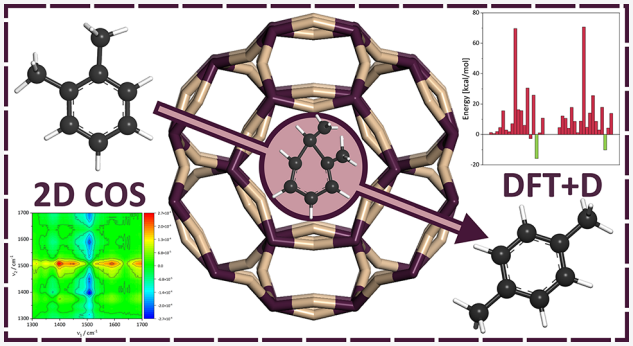

INTRODUCTION

Zeolites are crystalline aluminosilicates of high surface area and hydrothermal and thermal stability. Their structural properties responsible for the pores of molecular dimensions and the strong Brønsted and Lewis acid sites provide an advantage in the field of heterogeneous catalysis in many major chemical processes.[1,2] The expansion of the polymer industry in the last several decades forced the development of effective methods of polymer reactant synthesis. The *o*-xylene isomerization process was recognized as a feasible method of *p*-xylene synthesis. Among the three isomers of xylene, *p*-xylene is the most desirable industrial raw material due to its high demand in the manufacturing of terephthalic acid in the polymer (PET) industry.[3] The xylene isomerization reaction can serve also as a model reaction for characterizing the acidity in terms of the number, strength, and location of acid sites and porosity of aluminosilicates as well.

The most successful in xylene isomerization, thus industrially common, zeolites are protonic MOR[4] and ZSM-5[5] and, to the less extent, FAU[6] and FER.[7] The isomerization and disproportionation of *m*-xylene over the BEA samples with Si/Al ∈ [11, 42] were studied by Pérez-Pariente et al.,[8] and they concluded the Si/Al ratio being the decisive factor in the activity toward the isomerization and disproportionation activity (decreasing with increasing Al concentration). The maximum activity was found for Si/Al ca. 14−15, with a constant p-/o-ratio. The isomerization of xylenes in the wide-pore zeolites (FAU and MOR), with the use of isotopically labeled (deuterated) *p*-xylene, was also studied experimentally by Corma et al.,[9] who pointed out the discrimination of the mechanism, namely, that on both FAU and MOR, the uni- and bi-molecular isomerization mechanisms can take place, while on BEA, only the unimolecular 1,2-methyl shift can be observed. In the case of ZSM-5, it was found[10] that the isomerization of xylenes follows the intramolecular mechanism catalyzed by the Brønsted acid sites (B.a.s.), and the catalytic activity depends on the concentration of reactants on the acid sites which is, in turn, affected by diffusion. They also point out that the B.a.s activity depends also on its local environment. The important influence of diffusion on both activity and selectivity for xylene isomerization in ZSM-5 was demon-

Received: February 12, 2021
Revised: April 20, 2021
Published: May 5, 2021

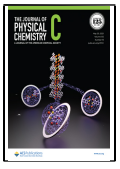

https://doi.org/10.1021/acs.jpcc.1c01307
J. Phys. Chem. C 2021, 125, 10334−10348

strated much earlier,[11−13] where the transition-state selectivity for *m*-xylene isomerization and its lower diffusivity raising the selectivity toward *o*- and *p*-xylenes were shown. Very comprehensive studies were provided by Min et al.[14] and others. The overall results of this study provide clear experimental evidence that product shape selectivity is responsible for the high *p*-xylene selectivity found in some medium-pore zeolites, whereas it is distinguishable from transition structure shape selectivity. The latter is ruled by the bimolecular and unimolecular mechanisms of isomerization. The intermediate's formation energy is only one of the factors influencing the overall catalytic activity.

In this respect, the recent research work in our group was dedicated to providing an insight into the *o*-xylene isomerization process over the 10-ring zeolites of the different pore connectivities and various steric constraints.[15−18] Based on the advanced rapid scan FT-IR measurements and the two-dimensional correlation spectroscopy analysis (2D COS) of the resultant spectroscopic data, it was possible to identify, during the *o*-xylene isomerization, the intermediate species characterized by the IR bands at 1485 and 1455 cm^{-1}. This method also allowed us to evaluate the mechanism of xylene isomerization over different zeolite structures and sequential order of events on the catalyst's surface. Also, based on the 2D COS analysis, the mechanism of xylene isomerization over different zeolite structures and sequential order of events on the catalyst's surface were evaluated. The formation of intermediates was found to be dependent on the rigidity of the microporous environment. Moreover, the formation of *p*-xylene in particular was directly associated with the presence of newly identified intermediate species and their accumulation in the rigid microporous environment. The structure of the intermediate species remained, however, unknown. The possible transformation of xylenes undergoing protonation includes either the route of insertion of the methylene group into the ring, thus forming the 7-membered ring product, or the paring reaction, where the 5-membered ring intermediate compound is formed.[19] Xylenes can be also produced in a feasible non-petroleum route of the alcohol-to-aromatics processes, where methanol or ethanol is converted into aromatics preferably with the high *p*-xylene content. The conversion of alcohols during the upgrading of natural resources (biomass and natural gas) to aromatics emerges as an interesting alternative of crude oil processing.[20,21] The conversion of methanol is investigated comprehensively, but also, ethanol conversion over acidic zeolites is gaining attention rapidly.[22−24]

The ethanol conversion to the C_{3+} hydrocarbons has been recognized to proceed through a dual-cycle mechanism[25] corresponding to the one established for the methanol-to-olefin process.[21] This aromatics-based mechanism proposes that the catalytically active sites are the organic−inorganic hybrids of cyclic organic species and zeolite acid sites. The methylation reaction proceeds with the use of the reactive organic species bound to the zeolite active site, which is followed by the elimination of products, thus regenerating the initial organic adsorbate.[26−29] Further similarities between the methanol and ethanol conversions to higher hydrocarbons are the distributions of formed products.[25,30−32] Additionally, the participation of xylenes in the alcohol-to-hydrocarbon process has been studied by Svelle et al.[33] The proposed methylation of toluene by DME led to *p*-xylene and methanol as one of the possible steps in the hydrocarbon pool mechanism. Since the methanol and ethanol conversion most probably proceeds through similar paths, understanding the ethanol conversion process can provide significant insights into the methanol-based route. The influence of aromatics on the methanol conversion reaction was first proved by Mole et al.[34,35] The addition of a small amount of toluene or *p*-xylene resulted in an enhanced conversion rate.[21] The participation of xylenes in the hydrocarbon pool mechanism prompted our search on similarities in results of the FT-IR spectroscopic observations of both processes. The origin of the 1485 cm^{-1} band was identified as an intermediate in the xylene isomerization process since its participation in the ethanol conversion process, presented in this article, was even more stimulating. The necessity of their assessment through the quantum chemical modeling emerges.

In the present article, several intermediate structures (namely, the 5- and 7-membered rings) and parent *o*-xylene, together with their IR spectra, were proposed and verified. As the FT-IR spectroscopy supported by 2D COS allowed us to gain significant insights into the xylene transformation process, the same methodology was applied to follow the changes in FT-IR spectra during the ethanol conversion process. The 2D COS analysis, developed by Noda,[36] is herein coupled with standard and rapid scan time-resolved in situ FT-IR spectroscopy. The tracking of the slightest changes in the FT-IR spectra of the catalyst surface during the reaction and the detection of intermediate products are possible.

EXPERIMENTAL SECTION

Materials. The NH_4ZSM-5 zeolite with a Si/Al ratio of 12 was purchased from Zeolyst Int. (CBV 2314). The protonic form of ZSM-5 zeolite was obtained by calcination under static air at 580 °C for 3 h with a heating rate of 1 °C/min; the *β* parent zeolite ($NH_4\beta$) was purchased from Zeolyst (CP814C). The native MOR zeolite was bought also from Zeolyst International, (CBV 10A). Chabazite was bought from Clariant. The TNU-9 zeolite was synthesized using 1,4-bis(*N*-methylpyrrolidinium)butane dibromide (1,4-MPB) as a template formed in situ by reaction between 1,4-dibromobutane (1,4-DBB) and 1-methylpyrrolidine (1-MP). In a typical synthesis, the final gel contained 4.5 (1,4-DBB)/13.5 (1-MP)/11 (Na_2O)/0.5 (Al_2O_3)/30 (SiO_2)/1200 (H_2O). The gel was stirred at room temperature for 1 h and then transferred to Teflon-lined 35 mL autoclaves. The synthesis proceeded at 160 °C for 8 days under agitation and autogenic pressure. The solid products were recovered by filtration, repeatedly washed with water, and then dried overnight at 100 °C. All hydrocarbons (from Sigma-Aldrich) used in this study were of 99% purity.

FT-IR Spectroscopy Studies. The self-supporting discs of studied samples were prepared (ca. 5 mg/cm^2) and evacuated in a quartz cell with CaF_2 windows at 530 °C under vacuum for 60 min. The adsorption of carbon monoxide (CO) was performed at −100 °C and that of ammonia (NH_3) was performed at 170 °C.[37,38]

Acid strength of sites was determined in CO adsorption and NH_3 thermodesorption experiments. The formation of a hydrogen bond between CO and the bridging hydroxyls of the original Si(OH)Al band in zeolites is responsible for the down shift of the band ($\Delta\mu_{OH\cdots CO}$). The higher the strength of the acidic proton in the Si(OH)Al unit, the higher the down shift is observed. The acid strength detection in NH_3 thermodesorption is performed as follows. In the first stage

https://doi.org/10.1021/acs.jpcc.1c01307
J. Phys. Chem. C 2021, 125, 10334−10348

of the experiment, all acid sites were neutralized with ammonia, while physisorbed molecules were removed by evacuation at 170 °C. In the second step, desorption was carried out at the two following temperatures: 330 and 450 °C. The ratios A_{330}/A_{170} and A_{450}/A_{170}, where A_{170}, A_{330}, and A_{450} are the intensities of the NH_4^+ band (1450 cm^{-1}) measured after each desorption step, were taken as the measure of the acid strength of protonic sites.

Sorption of *o*-xylene (analytical grade, 99% purity) on the zeolite samples (ca. 45 mg) was performed at 250 °C. The materials were contacted with *o*-xylene vapor (4 Torr = 0.53 kPa); the reaction was proceeded for 15 min, and then, the temperature was lowered to RT, and spectra were collected. Sorption of ethanol (40 Torr = 5.3 kPa) on the zeolites was also carried out at 250 °C. The spectra were collected for 120 min every 8 s. The analysis of spectra has been divided into two separate stages of reaction before and after 10 min from the reaction beginning. Two-dimensional correlation spectroscopy was performed over recorded 1D spectra in these two time domains.

All the spectra were recorded with a Bruker Vertex 70 spectrometer equipped with an MCT detector. The spectral resolution was 2 cm^{-1}. The 2D COS graphs were prepared with the use of OPUS 3D software from Bruker Optics and OriginPro 9.1.

Computational Details. All the quantum chemical calculations of energies, geometries and vibrational analyses were performed with the use of the DMol3[39] code at the periodic DFT level of theory, with the RPBE[40,41] correlation-exchange functional. This functional was chosen based on the conclusion that it is a good compromise in many cases when gas-phase molecules and solids are treated simultaneously, particularly because it provides a better description of the hydrogen bonds than PBE or revPBE. The orbitals were expanded in the basis set of DND quality with the DSPP pseudopotentials.[42] A basis set spatial cutoff distance of 4.5 Å was set and, as a convergence accelerator, the Gaussian smearing with a window width of 5×10^{-3} Ha was used. The SCF convergence criterion was set to 1×10^{-6} Ha, whereas for geometry optimization the convergence criteria were as follows: for the energy change between two successive iterations the value of 2×10^{-5} Ha was used, for the gradient norm the threshold of 4×10^{-3} Ha/Å was applied, and for the maximal atom displacement the value of 5×10^{-3} Å was used. Due to the large unit cell size of ZSM-5, MOR, and TNU-9, the Γ-point-only sampling of the IBZ (irreducible part of the first Brillouin zone) was found to be sufficient. For smaller unit cells (CHA), however, the IBZ was sampled due to the Monkhorst–Pack algorithm with a *k*-point density of 3 × 3 × 3. In all cases, the *k*-point separation in the reciprocal cell was sufficient, taking into account the calculations of the time-consuming vibrational analysis, ca. (0.05 × 0.05 × 0.07) $Å^{-3}$, (0.06 × 0.05 × 0.13) $Å^{-3}$, and (0.10 × 0.10 × 0.10) $Å^{-3}$, in the case of ZSM-5, MOR, and CHA zeolites, respectively (denser than the *rule-of-thumb* recommended value: 0.05 × 2π/Å for insulators). The London dispersion effects, important for the description of the zeolite–hydrocarbon interactions,[43,44] were accounted for by the semi-empirical correction to the DFT functional in a post-SCF manner, using the pairwise interatomic interactions dependent also on the charge density.[45] The unit cell parameters were optimized by fitting the energy–volume relationship to the Birch–Murnaghan equation of state.[46]

The stable geometries for each postulated reaction elementary step were determined with the use of the BFGS algorithm.[47,48] The (vibrational) entropic contributions were calculated via the classic, harmonic vibrational analysis, and the Gibbs free energies were calculated at T = 298 K, at the same temperature at which the spectra of gaseous and adsorbed species were recorded. The transition states were located starting with the LST/QST guess,[49] followed by the BFGS[50] refinement, and then verified by the vibrational analysis, under the condition of only one negative Hessian eigenvalue appearing among the calculated normal vibrations. The atomic charges and bond orders were obtained within the Hirshfeld[51] and Mayer[52] analyses, respectively.

Models. *Distribution of Al Sites.* Based on the experimental value of Si/Al, the number of aluminum atoms per unit cell was determined as follows: 6 out of 96 in MFI, 4 out of 64 in BEA, 3 out of 12 in CHA, 5 out of 48 in MOR, and 14 out of 192 in TNU-9 (Table 1). It is generally assumed

Table 1. Si/Al Values and the Channel Member Ring Count of the Studied Zeolites

zeolite	BEA	CHA	MFI	MOR	TNU-9
MR	12	8	10	12/8	10
Si/Al	15	3	15	8.6	14

that the aluminum atoms in zeolites are not distributed randomly but also not periodically; thus, their localization is not unambiguously assessed and is difficult to determine. Some information on aluminum distribution is, however, available for BEA,[53] MFI,[54,55] CHA,[56] MOR,[57] and TNU-9;[58] namely, for BEA, the preferable localization of Al is T5, for CHA—T1, for MFI—T10, T7, and T12, for MOR—T3, and for TNU-9—T2, T8, T11, T14, and T21, and these positions were exchanged by Al in this work. The location of aluminum and OH groups may be found in Figure 1. In our models, Al atoms are isolated except for BEA, so they should be referred to experiments for either zeolite of small amounts of Al pairs (ZSM-5(S)) or for high-acidic OH groups.[59] The OH groups have been located at the positions adjacent to the Al atoms. The OH group interacting with the *o*-xylene molecule has been chosen based on the accessibility, so that it points into the largest void possible, namely, into the channel (or the widest channel, if the channels of various sizes exist).

RESULTS AND DISCUSSION

FT-IR Studies of Ethanol Transformation over ZSM-5 Zeolite. The FT-IR spectra of ethanol transformation at 250 °C in ZSM-5 are presented in Figure 2. At the first stage of the reaction process, the formation of ethylene (2990 and 1888 cm^{-1}) is observed, which is next transformed into the higher hydrocarbons. The water molecules generated at elevated temperature of performed reaction are not able to adsorb on the Si(OH)Al, and water is detected only in the gas phase.

The complex nature of the undergoing ethanol-to-hydrocarbon (ETHs) process was investigated with 2D COS analysis. The overlapping of the diagnostic bands and the formation of various intermediates and products of reaction make the analysis of spectra challenging. The 2D COS analysis of collected spectra in the asynchronous mode allowed us to establish also the sequential order of events taking place on the catalyst surface. The 2D contour maps with the levels of changes in spectra are presented with two axes for wave-

https://doi.org/10.1021/acs.jpcc.1c01307
J. Phys. Chem. C 2021, 125, 10334–10348

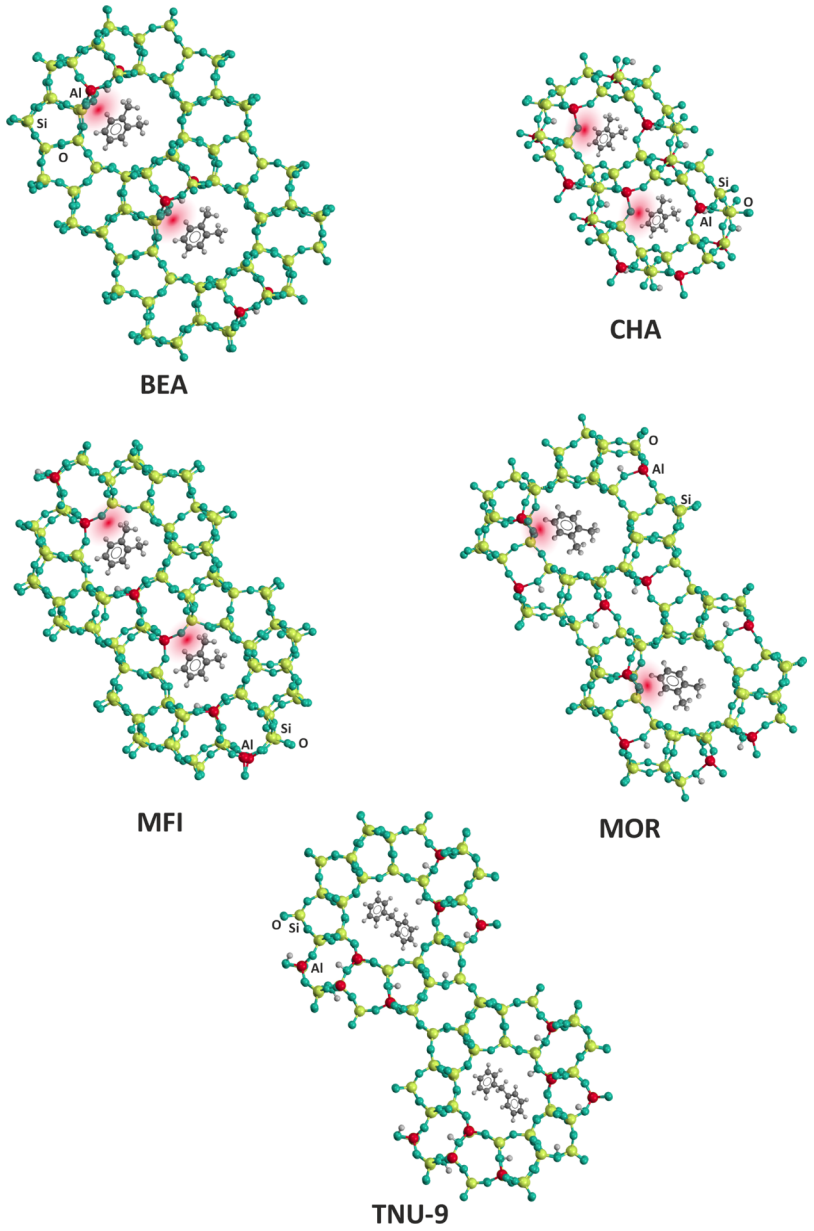

Figure 1. Optimized *o*-xylene molecule positions together with the location of the OH group (red clouds) in the channels of BEA, CHA, MFI, and MOR (first two rows) together with the optimized position of DFM in the channel of TNU-9. The linear scale of distances is preserved among structures.

numbers and one for the correlation level. The 2D maps possess much sharper and easier resolved peaks than the parent 1D spectra and can provide valuable insights into the following surface reactions.

The scrutiny of undergoing reaction was performed for two separate time domains: before (Figure 3) and after 10 min (Figure 4) from the introduction of ethanol. Synchronous maps of 2D COS analysis provided information on the direction of changes in the bands' intensities. First, the negative correlations of the 1507 and 1485 cm^{-1} bands and between 1485 and the set of bands, denoted hereafter with ampersand, 1588 and 1375 cm^{-1} were found. The band transformation, one into another, represented by abovementioned negative correlations, is accompanied also by the positive correlation, that is, the simultaneous changes in band intensities in the same direction. The positive correlations during the first 10 min of the reaction are found between 1507 cm^{-1} and 1588 and 1495 and 1474 and 1375 cm^{-1} bands (Figure 3A). The asynchronous maps provide information on the sequential order of events occurring on the zeolite surface during the reaction. Based on the analysis of the asynchronous map (Figure 3B), it can be inferred that the increase in the 1375 cm^{-1} band was followed by the increase in the 1507 cm^{-1} band, and then, the 1485 cm^{-1} band decrease occurred. The next stage of the reaction process was described only by positive correlations on the synchronous map (Figure 4A), that is, 1600 and 1507 cm^{-1} and 1495 and 1474 and 1386 and 1375 cm^{-1} bands. The asynchronous map (Figure 4B) proved that the sequential order of band intensity changes is as follows: 1600 and 1495 cm^{-1} bands increase before the 1508 cm^{-1} band. The presence of the aromatic species, for example, polymethylated benzenes (the 1507 cm^{-1} band is typical of 1,2,4-trimethylbenzene) on the zeolite surface confirms that the aromatics-based hydrocarbon pool mechanism is occurring

https://doi.org/10.1021/acs.jpcc.1c01307
J. Phys. Chem. C 2021, 125, 10334−10348

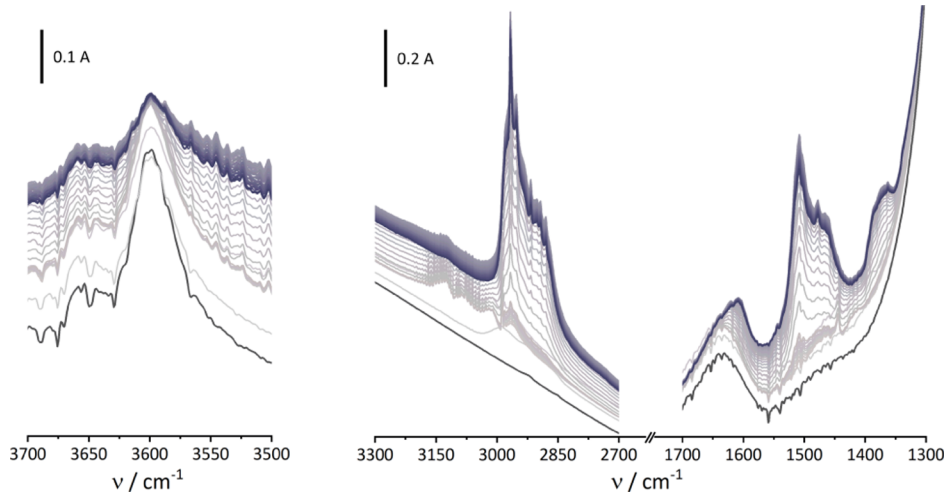

Figure 2. Red lines: FT-IR spectra of ethanol adsorbed in ZSM-5 successively collected at 250 °C every 5 min of reaction; dark gray line: spectrum of activated ZSM-5 before the sorption of ethanol.

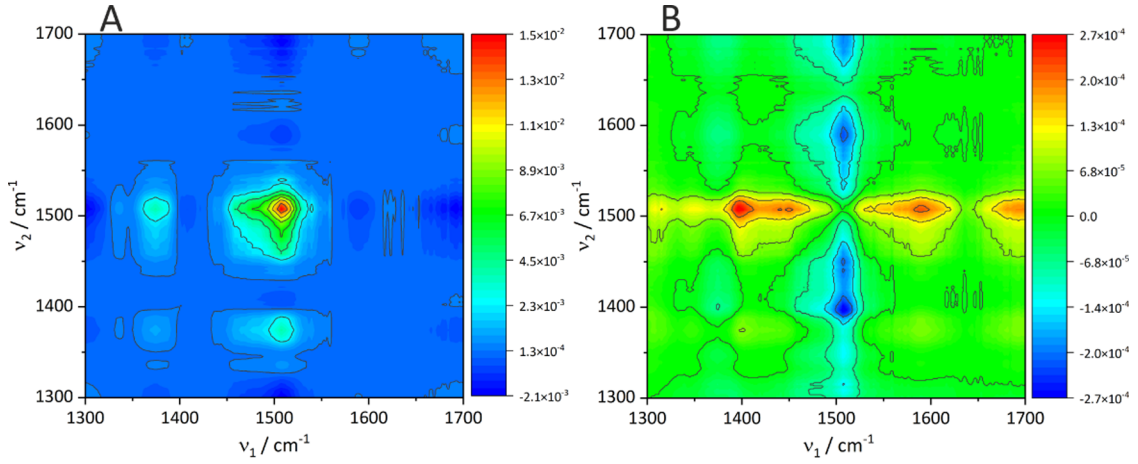

Figure 3. 2D correlation maps (A—synchronous, B—asynchronous) in the CH_x bending vibration region for the ETH reaction for the first 600 s of the process at 250 °C.

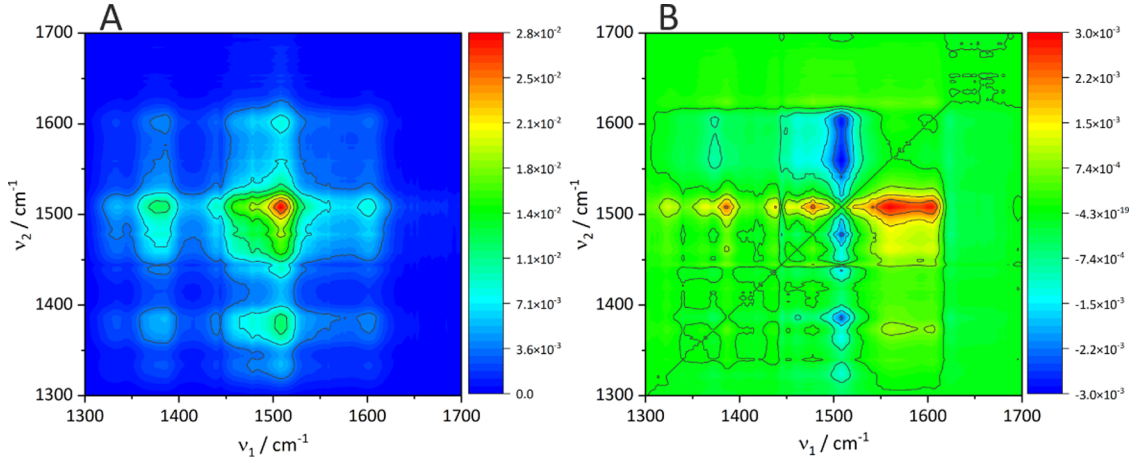

Figure 4. 2D correlation maps (A—synchronous, B—asynchronous) in the CH_x bending vibration region for the ETH reaction after 600 s of the process at 250 °C.

under our applied experimental conditions. Besides 1,2,4-TMB, also, benzene (1474 cm^{-1} diagnostic band) and toluene (1495 cm^{-1} diagnostic band) can be identified during the reaction process. Most importantly, the 1485 cm^{-1} band of intermediate species found during the xylene isomerization process has been identified also during the ETH process, and the 2D COS analysis confirmed its transformation into the 1507 cm^{-1} band representative for 1,2,4-TMB. Previously, it

https://doi.org/10.1021/acs.jpcc.1c01307
J. Phys. Chem. C 2021, 125, 10334−10348

was shown that in the TNU-9 zeolite, even in the lower temperature region, the formation of polymethylated benzenes occurred;[17] the ZSM-5 zeolite requires, however, higher temperatures for 1,2,4-TMB observation during ethanol transformation. The discrimination between the 1,2,4-trimethylbenzene and 1,2,4-triethylbenzene under our experimental conditions is highly difficult, as IR spectra of both show high similarities; thus, it must be taken into account that even if the products of the ETH and mETH process are identical, the intermediates may differ with some preferences to polyethylated benzenes when ethanol is considered. The accumulation of reaction products in the second part of the process and lack of negative correlations suggest that the hydrocarbon pool initiation was finalized, and steady-state reaction products, partially accumulated on the surface, are in majority realized to the gas phase. The formation and accumulation of the aromatic species are observed as abovementioned positive correlation between the set of bands (1600 & 1507 and 1495 & 1474 cm^{-1}); this is also accompanied by a relatively high correlation level from C−H bending vibrations bands (1386 and 1375 cm^{-1}) (Table 2).

Table 2. IR Band Assignment

band position in cm^{-1}	assignment
2990, 1888	ethylene in the gas phase
2740	intermediate: methylbenzenium ion (aromaticC−H stretching)
1600, 1588	condensed aromatic species
1507	1,2,4-trimethylbenzene (C−C stretches in the aromatic ring)
1495	toluene (C−C stretches in the aromatic ring)
1485	intermediate: xylenium ion
1474	benzene (ν_{19} C−C vibration of the aromatic ring)
1455	intermediate: diphenyl methane (scissoring vibration of CH_2)
1386, 1375	C−H_x bending modes

FT-IR Studies of *o*-Xylene Transformation. Previously, it was proved that the microporous structures such as ZSM-5, IM-5, and TNU-9 deliver differentiated catalytic performance in methanol-to-hydrocarbon,[21,60] ETH,[17] and xylene isomerization processes.[15] The 2D COS analysis showed that the *o*-xylene transformation is strongly influenced by the diffusion of the reagents in a microporous environment. The formation of intermediate species characterized by IR bands at 1485 and 1455 cm^{-1} was recognized. The latter can be assigned to the scissoring vibration of CH_2 in diphenyl methane. Their amount was associated to the rigidity of the microporous system: the most spacious environment for *o*-xylene transformation was characterized by the lowest population of intermediates, whereas structures offering a sufficiently tight geometry accommodated intermediate species in higher quantities, finally leading to the production of *p*-xylene with high selectivity.[15] The analysis of the influence of the acid site location and its strength on the xylene isomerization process was also followed using the FT-IR spectroscopy and 2D COS analysis.[18] Among ZSM-5 zeolites of different Si/Al ratios, the isomerization reaction proceeded effectively over ZSM-5 zeolites of Si/Al between 10 and 30. The reduction of Brønsted acid site density, that is, the increase in Si/Al, enabled the disproportionation path (zeolites of Si/Al higher than 40). The formation of intermediate species was found to be induced by the diffusion constraints in 10-ring channels. The ZSM-5 zeolite among different zeolite structures was studied most extensively as highly suitable for xylene isomerization.

Diagnostic Band. The experimental FT-IR spectra and the vibrational analysis for the considered intermediates brought independent and compatible information, for example, the presence of the diagnostic band at ca. 1485 cm^{-1} (Figure 5).

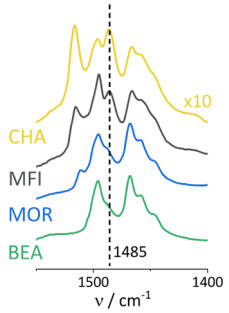

Figure 5. Intermediate's IR band upon *o*-xylene adsorption on CHA, MFI, **MOR**, and BEA.

Additionally, it was proved that the band at 2740 cm^{-1} is associated with the presence of the intermediate diagnostic band.[16] On the other hand, for both gas-phase and physisorbed *o*-xylene, the 1485 cm^{-1} band is not observed. The experimental Fourier transform infrared (FT-IR) spectra presented in this paper for several additional zeolite structures, CHA, MFI, MOR, and BEA, after the in situ isomerization of *o*-xylene (Figure 5) prove that the 1485 cm^{-1} band can be detected also in other zeolite structures. The smaller the cavity formed by intersecting channels (BEA, MOR, and MFI) or cages (CHA), the higher intensity of the 1485 cm^{-1} band detected in the IR spectra. The vibrational analysis for the gas-phase *o*-xylene molecule reveals the strong bands at ca. 1473 and 2939 cm^{-1}—none were found close to 1485 cm^{-1}. In the case of the physisorbed *o*-xylene, the strong bands occur at 1389 and 2975 cm^{-1} for MFI, at 1392 and 2955 cm^{-1} for MOR, at 1224 and 3052 cm^{-1} for CHA, and at 1411 and 2770 cm^{-1} for BEA.

In Table 3, the calculated bands at ca. 1485 cm^{-1} are gathered for all structures of zeolites and all considered intermediates which yield the diagnostic band. Only for the C5o structure, the band at ca. 1485 cm^{-1} appears for all studied zeolites, making this structure the most probable as an intermediate. Surprisingly, all structures have positive formation energy in mordenite, and still, C5o has the lowest energy. Taking into account, however, that bulkier (C7) intermediates cannot be formed in 8-membered channels (CHA), the C7-4 structure is possible for MFI, MOR, and BEA.

We have found that the 1485 cm^{-1} band corresponds to the deformation vibrations (e.g., 1486 and 1487 cm^{-1} bands in MFI are the CH_2 scissoring vibration of the CH_3 group). For CHA, the 1486 cm^{-1} band is the scissoring and twisting of the CH_3 group with the admixture of the ring deformation. Hence, the presence of the 1485 cm^{-1} band can be regarded as the indicator of the *o*-xylene protonation.

Structure of Intermediates. The total number of 18 hydrocarbon C5 and C7 candidates for being the intermediates in the intramolecular mechanism has been considered; their structures are presented in Figure 6.

https://doi.org/10.1021/acs.jpcc.1c01307
J. Phys. Chem. C 2021, 125, 10334−10348

Table 3. Resultant (DFT Calculated) IR Bands (Diagnostic, at ca. 1485 cm^{-1}, in the Range ± 10 cm^{-1}, in Parenthesis Bands of Very Low Intensity, Italic—Positive Low Formation Energy, Bold—Negative Formation Energy) for Postulated Intermediates in Studied Zeolites

	MFI	MOR	CHA	BEA
intermediate		wavenumber/cm^{-1}		
C5o	**1487**	1478	**1485**	**1482**
C5m	*1483*			
C7-1			1480	(1481)
C7-2		1482		1477
C7-3			1483	
C7-4	*1480*	1479		1488
C7-5		1486		1476
C7-9	1484		1477	
C7-9t	1480			
C7-10	1486		1486	(1487)
C7-11			1478	1487
C7-12	**1486**		*1488*	1491
C7-13	(1492)		1481	

Adsorption Energy. Adsorption of *o*-xylene leads to the protonated forms before it is transformed into other isomers. The energetic effect of forming such protonated xylenes (denoted hereafter as ΔE_f—electronic energy; ΔG_f—free energy at 298 K) can be decomposed into three components—the xylene protonation energy (ΔG_{pr}), the zeolite deprotonation energy (ΔG_{dp}), and the interaction energy (ΔG_{int})

$$\Delta G_f(Z, I) = \Delta G_{pr}(I) + \Delta G_{dp}(Z) + \Delta G_{int}(Z, I) \quad (1)$$

The contributions to adsorption energy are, to some extent, mutually independent as the protonation energy depends on the kind of intermediate "(I)" only and the deprotonation energy depends on zeolite "(Z)" only, while the energy of the interaction between zeolite and the protonated form of xylene depends on both zeolite and the intermediate structure "(Z, I)". Stabilization of a given intermediate is determined by the interplay between the stabilization effects: $\Delta G_{int} < 0$ and $\Delta G_{pr} < 0$ and endothermic effect $\Delta G_{dp} > 0$. The energy necessary to break the O−H bond is so high that proton transfer energy, $\Delta G_{tr} = \Delta G_{pr} + \Delta G_{dp}$, is always positive.

For the total adsorption energy to be negative or at least as low as possible, the energy of deprotonation should be relatively low, while, at the same time, the protonation energy and the energy of $C_8H_{11}^+$ cation interaction with the deprotonated zeolite should be relatively high to the absolute value (high stabilization). As will be discussed later, such a coincidence among approximately 75 considered systems is quite rare.

Protonation Energy. The stability of isolated considered intermediates (Figure 6) varies in quite a wide range (ΔG_{pr}, see Figure 7)—its variability between structures reaches about 50 kcal/mol (up to about 100 kcal/mol); thus, it gives the large contribution to the differentiation of the overall

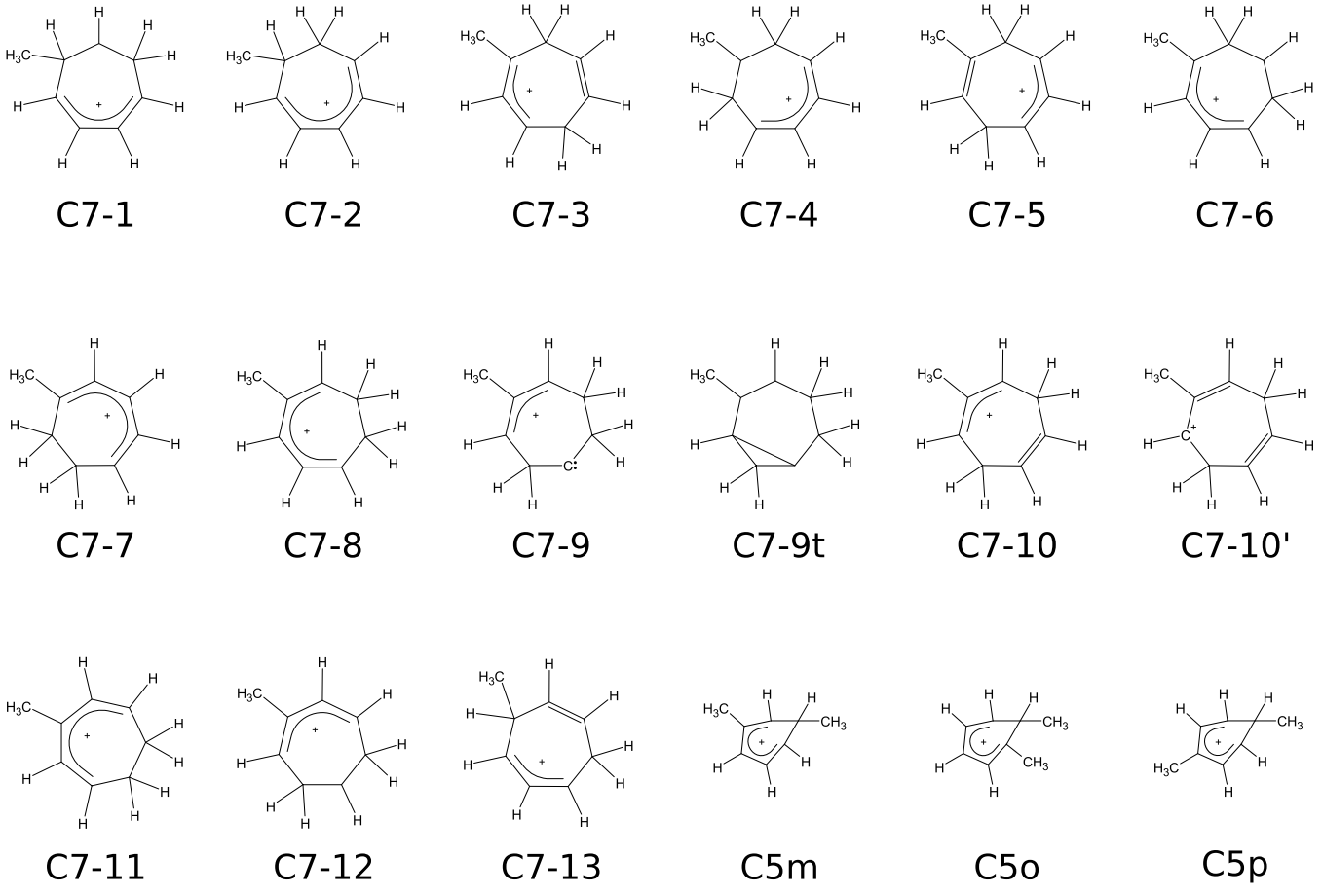

Figure 6. Sketch of the C7 and C5 intermediates considered in this article.

https://doi.org/10.1021/acs.jpcc.1c01307
J. Phys. Chem. C 2021, 125, 10334−10348

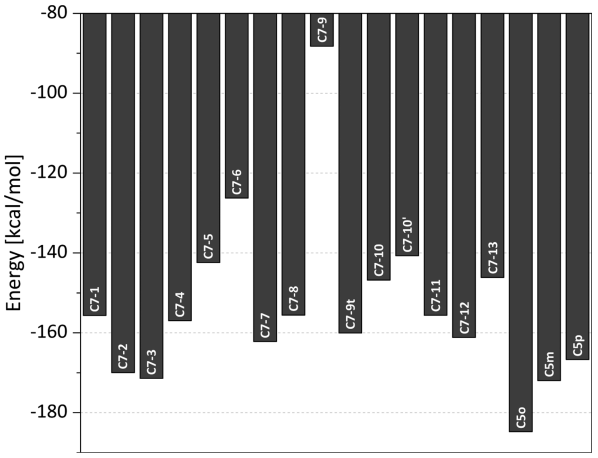

Figure 7. Calculated protonation energy, ΔG_{pr}, of *o*-xylene toward formation of different intermediates.

formation energy (ΔG_f). Based on the protonation energy, the candidates for intermediates can be indicated. Among the structures containing a pseudo-5-membered ring, the C5o structure is the most stable, while C7-2 and C7-3 are the most stable among the 7-membered ring structures. On the other hand, the C7-9 structure is definitely the least stable because one of the carbon atoms contains a lone electron pair.

Deprotonation Energy. As it was mentioned before, ΔG_{pr} does not depend on the zeolite structure, while the deprotonation energy, ΔG_{dp}, depends on zeolite only. The data concerning zeolite ΔG_{dp} parameters gathered in Table 4 are ambiguous. On one hand, there is a variety of measures of acidity, and on the other hand, the OH groups are heterogeneous due to the location and Al distribution. All experimental measures (Table 4) present the same trend: for zeolites without 8-membered ring channels, the acid strength relationship is MFI > BEA; for zeolites with 8-membered ring channels, the acid strength for CHA is higher than for MOR. The deprotonation energy, ΔG_{dp}, does not exhibit a very large diversity for the considered structures (ca. 6 kcal/mol).

Acid Strength Measures. The strength of acid sites can be assessed with the use of a few measures; often, they are the experimental ammonia desorption ratio, A_{330}/A_{170} (ratio of absorbance measured at 330 °C versus absorbance at 170 °C), and the OH band red shift upon CO adsorption ($\Delta\tilde{\nu}_{OH\cdots CO}$).

The former measure, A_{330}/A_{170}, should be, however, considered with due bias. Namely, the ammonium cation interacts very strongly with the zeolite framework oxygen, and the interaction is particularly pronounced in the structures consisting of 8-ring channels, for example, MOR and CHA (confinement effect, vide infra)—this is in line with our findings. Consequently, information on proton acid strength cannot be directly estimated from the A_{330}/A_{170} values, as an additional effect (confinement effect) contributes to the NH_4^+ ion stabilization. The A_{330}/A_{170} measure is indeed a superposition of three effects, as was said before: the deprotonation energy and the confinement effect.

The latter quantity, $\Delta\tilde{\nu}_{OH\cdots CO}$, is the downshift of the wavenumber of the OH stretching band upon adsorption of CO. However, the measured and calculated enthalpy points toward MFI as the least acidic. The obtained results are in line with those obtained by Boronat and Corma,[61] who also note that the discrepancies between different acidity measures do not prejudge their usability since those measures are prone to other factors such as the channel size or structure, which contribute to the overall effect of confinement.

The confinement effect, introduced by Derouane et al.,[62] assumes the influence of the curvature of the zeolite pores and cages on the reactivity via the long-range dispersion interaction. This effect is contrary to the shape selectivity (with respect to the reactants, products, or transition structures), which rather stems from the short-range Pauli repulsion.[63] It can rationalize the observation that mordenite and chabazite, having 8-membered ring channels, show overestimated values of adsorption energy, both computed and registered experimentally, compared to MFI and BEA, despite the former's lower acid strength.

The recent computational work of Iglesia[64] reviews a plethora of articles and discusses the reactivity descriptors as being determined by the properties of both acid sites and adsorbed molecules. The properties actually concern the proton donor and acceptor properties. This is criticized by the authors, and the necessity of inclusion of energy-minimizing charge reorganization is emphasized. The importance of the confinement effect, as the tendency of the guest and host to undergo the electrostatically driven mutual geometrical fit, even at the expense of the reorganization energy, is also accented.

In this spirit, the more detailed decomposition of the acid site−molecule interaction is performed.

As was pointed out by Boronat and Corma,[61] some bases can be used to "measure" the acid strength of the centers if the different proton affinity is taken into account. Indeed, for a selected set of intermediates, here, six out of 18 (see Figure 8) heat formations depend mainly on proton affinity due to the similar confinement effect. It cannot be, however, regarded as a general rule for intermediates (even those of similar size). Taking into account that ΔG_{dp} is almost constant, the deviation of heat formation is essentially due to ΔG_{int} values (see Figure 9). The described dependencies indicate that the acidity of centers which protonate xylene molecules rises in the sequence of MFI ≈ CHA < BEA (in Figure 9 the acidity rises from the left top corner toward the right bottom corner).

Table 4. DFT + D Deprotonation Energies (Gibbs Free Energy ΔG_{dp} at T = 298 K, Adiabatic Energy ΔE_{dp}^{v+r}, Vertical Energy ΔE_{dp}^{ver}, Relaxation Energy ΔE_{dp}^{rel}), and the Vertical Electron Detachment Energy ΔE_{ved} (Negative Electron Affinity), Calculated for Studied Zeolite Models[a]

	ΔG_{dp}	ΔE_{dp}^{v+r}	ΔE_{dp}^{ver}	ΔE_{dp}^{rel}	ΔE_{ved}	$\tilde{\nu}$/cm^{-1}	rOH/Å	α/deg	r_{Al-Al}/Å
MFI	248	251	282	−31	**168**	3587	0.987	138.0	4.45
MOR	249	255	283	−28	**162**	3560	0.988	136.0	7.15
CHA	243	250	274	−24	**164**	3595	0.987	134.0	6.35
BEA	247	253	284	−31	**172**	3521	0.991	132.7	4.93

[a]The letter α denotes the ∠(Al−O(H)−Si) angle. All energies are in kcal/mol.

https://doi.org/10.1021/acs.jpcc.1c01307
J. Phys. Chem. C 2021, 125, 10334−10348

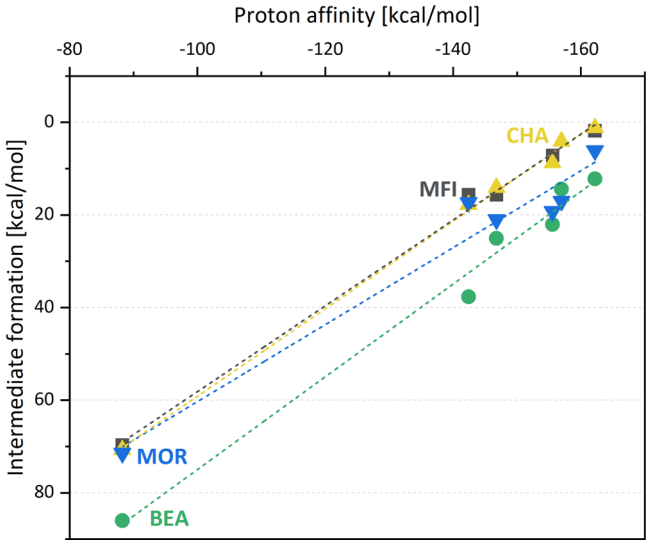

Figure 8. Correlation between the formation energy and protonation energy of *o*-xylene transformation intermediates. The C7 structures, in the order from the lowest to highest proton affinity: C7-9, C7-5, C7-10, C7-8, C7-4, and C7-7, are presented. Inspired by ref 61.

Similar conclusions can be inferred from the magnitude of $\tilde{\nu}$ (lowest for BEA) and r_{OH} (highest for BEA), see Table 4, which indicates their adequacy as the measure of acid strength.

The deprotonation energy (ΔE_{dp}^{v+r}) can be decomposed into two contributions: the vertical proton detachment (ΔE_{dp}^{ver}, proton detachment without relaxation of the rest of the system) and the relaxation energy (ΔE_{dp}^{rel}, geometry change energy imposed by deprotonation). The values of the Gibbs free energy (vibrational entropy), the adiabatic energy, the vertical energy, and the relaxation energy are also gathered in Table 4.

ΔE_{dp}^{ver} can be considered as a measure of the energy barrier in the detachment of the proton process (despite the fact that after detachment of H^+, the structure relaxes) and, in that way, a measure of acid strength. To the best of our knowledge, neither ΔE_{dp}^{ver} nor ΔE_{dp}^{rel} has been used for the estimation of acid strength in zeolites before. It seems, however, justified as the quantity ΔE_{dp}^{ver} was successfully used for the calculation of the acidic dissociation constants in solutions.[65] The vertical energy of deprotonation changes in a broader range than ΔG_{dp} and is the lowest for CHA, while the ammonia adsorption energy is the highest for this zeolite, indicating the overwhelming impact of the confinement effect on the ammonia stabilization. The relaxation energy (ΔE_{dp}^{rel}) compensates significantly the variation in ΔE_{dp}^{ver}—the higher ΔE_{dp}^{ver}, the higher value of ΔE_{dp}^{rel}, and hence ΔE_{dp}^{v+r} and ΔG_{dp} are very similar for different zeolites. Experimental acid strength measure (ammonia desorption ratio, A_{330}/A_{170}) and the OH band red shift upon CO adsorption ($\Delta\tilde{\nu}_{OH\cdots CO}$)[18] correlate well with the ∠(Al−O(H)−Si) angle (Table 5).

The following factors could be identified as influencing the Brønsted acid strength: (i) the local structure of the center and (ii) the interaction with the channel wall, namely, with wall oxygen atoms located above the adsorbed molecule (in the framework orientation when the OH group is located at the bottom of the channel)—the effect "from the top".[70] Some properties, for example, ∠(Al−O(H)−Si), are relevant for the local properties, while the other are for the overall effect. The "from the top" interaction modulates $\tilde{\nu}$, which increases due to the increased polarization of the OH group.[70] It is also affected by the distance between the Al−OH group and the closest Al atom (r_{Al-Al}); thus, in the case of MFI, $\tilde{\nu}$ for the OH group adjacent to the Al site is blue-shifted because of its proximity to the next Al, what stems from the high "local concentration" of Al sites (low Si/Al ratio). In the case of BEA, however, contrary to the effect of the small ∠(Al−O(H)−Si) angle, the low $\Delta H_{ads}(NH_3)$ energy, and the short r_{Al-Al} distance, this zeolite has unexpectedly low $\tilde{\nu}$ and long r_{OH} distance, what can be rationalized by the "from the top" effect, namely, the interaction with zeolite framework walls.

The energy of the vertical electron detachment from the acid residue, ΔE_{ved} (negative electron affinity), discussed in the literature as the measure of the acid strength of strong acids and superacids,[71,72] does not discriminate, however, studied zeolites relevantly. The protonation of xylenes requires the acidic property of the zeolite, and all of the considered zeolites are acidic enough to protonate *o*-xylene, and the other factors determine the prevailing path of the reaction. The OH group **strength** cannot be, therefore, regarded as the determining factor in the isomerization process in studied zeolites.

Interaction Energy. The last component of the formation of the intermediate, according to eq 1, is the energy of the interaction of the $C_8H_{11}^+$ cation with the anion of the zeolite framework, $\Delta E_{int}(Z, I)$, which depends on the structure of both the cation and zeolite (Figure 9).

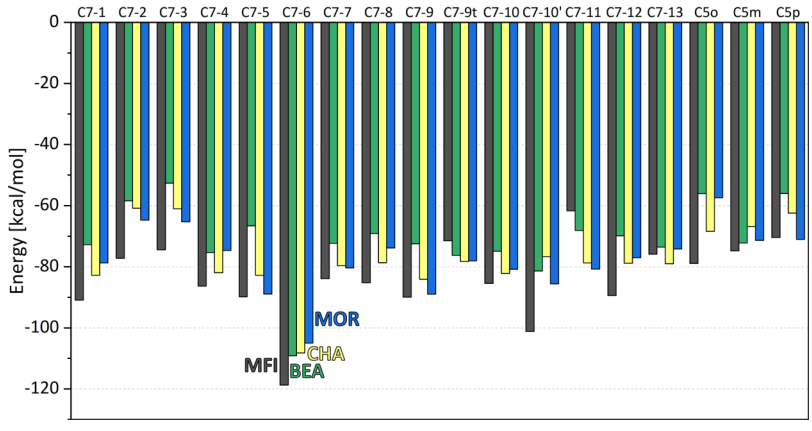

Figure 9. Interaction energy of possible intermediates and the zeolite anion.

https://doi.org/10.1021/acs.jpcc.1c01307
J. Phys. Chem. C 2021, 125, 10334−10348

Table 5. Experimental NH_3 Adsorption Enthalpy, $\Delta H_{ads}(NH_3)$, NH_3 Desorption Ratio, A_{330}/A_{170} and A_{450}/A_{170}, and the OH Band Red Shift Upon CO Adsorption, $\Delta\nu_{OH\cdots CO}$

	$\Delta H_{ads}(NH_3)$	A_{330}/A_{170}	A_{450}/A_{170}	$\Delta\tilde{\nu}_{OH\cdots CO}/cm^{-1}$	$\tilde{\nu}_{OH}/cm^{-1}$
MFI	−34.7[66]	0.91	0.20	315	3603
	−34.6[67]				
MOR	−38.3[66]	0.6 +	0.35	309	3600
	−41.8[68]				
CHA	−32.3[69]	0.78	0.45		3610, 3565
BEA	−30.8[69]	0.5	0.15	309	3609

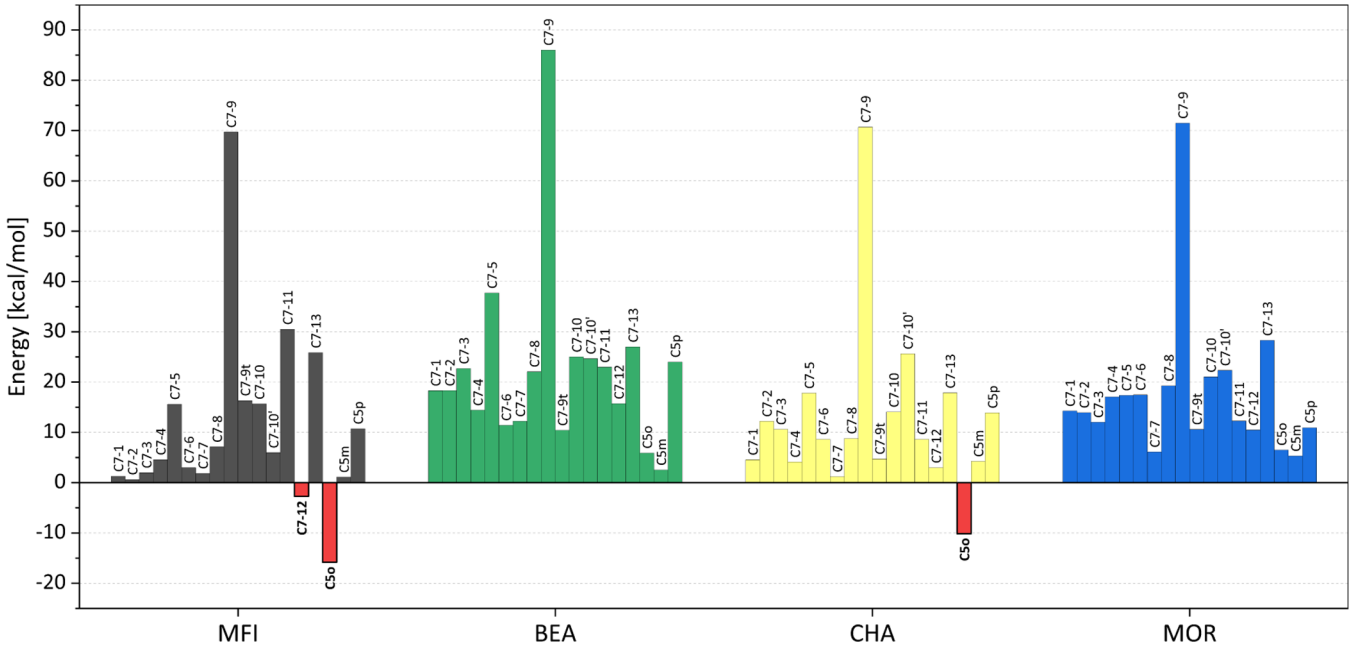

Figure 10. Formation energy, ΔE_f, (defined according to eq 1), of possible C5 and C7 intermediates in studied zeolites (silicalite forms). The negative value means a stable structure.

Adsorption Energy—Summary. As it was mentioned before, the factors other than the strength of Si(OH)Al sites determine the prevailing path of the reaction. It can be seen that the cation structure has a greater impact on $\Delta E_{int}(Z, I)$. This variation, however, is compensated to a large extent by the protonation energy. This becomes noticeable after adding up all the contributions (Figure 10)—the differentiation of the overall energy, among 18 intermediates, is lower than when considering particulate energy components. In this case, the total energy for the C7-9 structure is also the most unfavorable. In most cases, the intermediate formation energy, ΔE_f, reaches about 5−20 kcal/mol. For some combinations of the intermediate andzeolite, however, the value of the formation energy is close to zero, including C7-1, C7-2, C7-3, C7-6, C7-7, and C5m in MFI and C7-7, C7-9t, C7-12, and C5m in CHA, and for several cases, it reaches negative values: C5o in MFI, BEA, and CHA and C7-12 in MFI. Still, the intermediate products are only weakly stabilized in the wide-pore structures (MOR and BEA), and consequently, the 1485 cm^{-1} bands are weak or even absent (Figure 5). The C5o intermediate is most stable in MFI and CHA; however, for the latter, the diffusion limitation is critical. In the 12-MR zeolites, additionally, another intermediate can be postulated, namely, C7-12 (see Figure 11).

The formation energies, averaged over all structures, indicate that they are similar to each other for MFI and CHA (they are also the lowest), higher for MOR, and the highest for BEA zeolite: 10.7, 12.3, 17.6, and 22.3 kcal/mol, respectively. It is correlated with the size of the pores—BEA zeolite has 12-membered ring channels, and MOR has both 12- and 8-membered ring channels, while the access of xylenes to the MFI channels and the CHA cages is ruled by the 10- and 8-membered rings, respectively. Based on this analysis, it can be

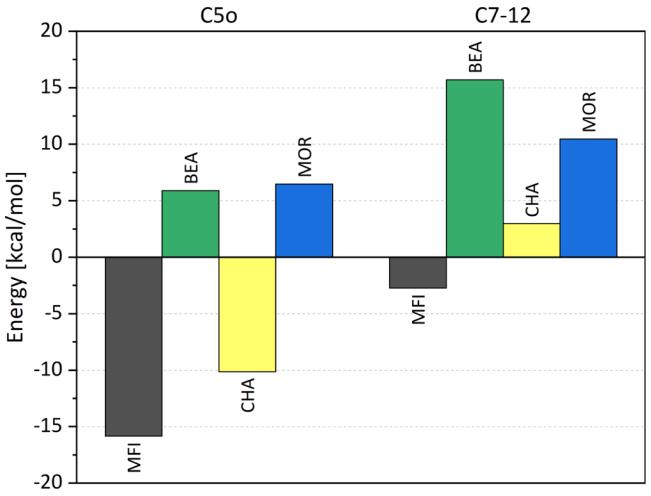

Figure 11. Formation energy of the most stable C5o and C7-12 intermediates in the studied zeolites.

https://doi.org/10.1021/acs.jpcc.1c01307
J. Phys. Chem. C 2021, 125, 10334−10348

concluded that the intermediate products are better stabilized in zeolites with a smaller pore structure. These results are also in line with IR experiment, namely, the band at 1485 cm^{-1}, attributed to the intermediate (Figure 5), has a high intensity for small pore zeolites such as CHA or MFI and low for large pore structures, MOR and BEA. CHA was chosen for modeling to show that *o*-xylene cannot fit into the channels, so, moreover, it cannot diffuse through the 6-MR windows in the structure. It is, however, possible to compare the experimental results to the computational results due to the interaction of the *o*-xylene molecules with the channel openings at the external surface of the zeolite grains. Still, such adsorbed structures yield the bands of only very weak intensities; thus, the relative intensities of the band at 1485 cm^{-1} were used in Figure 5 (the spectrum of CHA was multiplied by 10). Nonetheless, for the high-quality spectra, it is possible to register such bands above the noise level. Indeed, comparing the stabilization energies of *o*-, *m*-, and *p*-xylene in CHA, it can be seen that the former two isomers are much less stabilized, and they are also less stable compared to those in MOR and MFI (see Table 7).

Intermolecular Mechanism. In possible xylene isomerization pathways, the intra- or intermolecular mechanisms are usually taken into account. In the latter case, the diphenylmethane (DFM) molecule is considered the intermediate.[14] In the 10-ring or wider channels, the intermolecular mechanism is postulated. Indeed, MOR and BEA structures (with 12-ring channels) with DFM are energetically favored—all adsorption energies are negative (Table 6). Even DFM as a product is stable in all structures; the formation of DFM could be suppressed spatially in the zeolite with 10-ring channels.

Table 6. Sorption Energy (ΔE_{ads}), Gibbs Free Energy (ΔG_{ads}), and Description of Diagnostic IR Bands for DFM in Selected Zeolites[a]

	MFI	MOR	CHA	BEA	TNU
ΔE_{ads}/(kcal/mol)	−42	−53	−45	−59	−69
ΔG_{ads}/(kcal/mol)	−40	−54	−42	−63	*
$\tilde{\nu}$ close to 1455 cm^{-1}		**1456** (s)	1459 (vw)		1454
scissoring $\tilde{\nu}(CH_2)$/cm^{-1}	1455 (w)	1472 (m)	1488 (w)	**1457** (vs)	1453
stretching $\tilde{\nu}(CH_2)$/cm^{-1}	3041 (s)	2981 (s)	2919 (s)	2966 (s)	2956 (s)
	3133 (a)	3024 (a)	3005 (a)	3006 (a)	3000 (a)

[a]The labels "s", "m", "w", "vs", and "vw" denote strong, medium, weak, very strong, and very weak band intensity, respectively. Bands at ca. 1455 cm^{-1} are in boldface. In the case of TNU, the intensities have not been calculated. For stretching wavenumbers, the label "a" means asymmetric and "s" denotes symmetric vibrations.

The scissoring vibration of CH_2 at 1455 cm^{-1} is a diagnostic band of DFM. Vibrational analysis reveals the presence of the CH_2 band in the range between 1455 and 1488 cm^{-1} (Table 6). This band turned out to be relatively weak except for the case of BEA. Surprisingly, for MOR, another strong band appears at ca. 1455 cm^{-1}, stemming from the asymmetric vibration of the benzene ring, but it is not the case for MFI (it appears at 1439(m) cm^{-1}) or CHA (1459(vw) cm^{-1}). Based on this observation, it can be concluded that if the diagnostic band is present in the registered spectrum, it is the potential indication of the DFM presence, but the band in this region can also have a different origin. On the other hand, the CH_2 band could be too weak to be visible in the spectrum despite the presence of DFM in the sample (e.g., MFI). The experimental solution for the issue of the DFM formation in the studied system could be the adsorption of DFM at the temperature at which it does not react. Based on the DFT calculations, it can be predicted that the band at ca. 1455 cm^{-1} can be observed for DFM formed in MOR and BEA (boldface values in Table 6). In the case of TNU, the vibrational analysis was performed with partial Hessian (limited to the DFM molecule). Computed wavenumbers indicate scissoring vibration and are close to 1455 cm^{-1}. According to the calculations, for the DFM molecule adsorbed in TNU, at least two vibrations with wavenumbers close to 1455 cm^{-1} are observed (Table 6). The band intensities, however, have not been calculated, so more precaution should be taken due to the less-reliable computational methodology used, especially taking into account that TNU has pores as narrow as MFI (10-membered ring). Unfortunately, other intermediates can also contribute to the bands close to this wavenumber.

To conclude the issue of DFT, the computational study predicts that the presence of DFM in the zeolite structure yields the band at the diagnostic wavenumber for DFM in the case of MOR and BEA, but it cannot be reasoned in a reverse way, that is, that the band at ca. 1455 cm^{-1} can be a proof for the presence of DFM.

Taking into account the modeling and experimental results, at least some contribution of the intermolecular mechanism of xylene isomerization is highly likely in MOR and BEA zeolites. In an intermolecular reaction, however, one intermediate molecule is formed for every two consumed, so generally intramolecular reactions are more entropically favored (configurational entropy). Moreover, it should be emphasized that the possibility of an intermolecular mechanism does not preclude the participation of the intramolecular one.

Impact of Aluminum Presence. For the structures with a higher Si/Al ratio, the isomerization is less effective, and the transalkylation rather takes place, particularly on the outer surface of the grain. The sorption energies for the xylene isomers in both silicalites and zeolites with finite Si/Al are summarized in Table 7. In silicalites, the sorption energy rises in the sequence of BEA < CHA < MOR < MFI. In the aluminated forms, however, the sequence generally is less monotonous with 12-MR BEA presenting the weakest sorption, except *p*-xylene, where the sorption energy is

Table 7. Sorption Free Enthalpy of Xylenes in Silicalites and Zeolites with Finite Si/Al[a]

zeolite	MFI	MOR	CHA	BEA
Si/Al		∞		
		ΔG_{ads}/(kcal/mol)		
ortho	−27	−21	−16	−6
Meta	−21	−20	−15	−15
Para	−31	−35	−32	−26
Si/Al	15	8.6	3	15
		ΔG_{ads}/(kcal/mol)		
ortho	−20 (7)	−30 (−9)	−28 (−12)	−9 (−3)
meta	−34 (−13)	−23 (−3)	−20 (−5)	−8 (7)
para	−42 (−11)	−44 (−9)	−38 (−6)	−33 (−7)

[a]The energy difference imposed by the introduction of Al is given in the parentheses.

https://doi.org/10.1021/acs.jpcc.1c01307
J. Phys. Chem. C 2021, 125, 10334−10348

comparable to that of other zeolites. In silicalites, the sorption is strongest for *p*-xylene, while *m*- and *o*-xylenes give similar sorption energy with exception of wide-channel BEA where sorption of *o*-xylene is very weak.

The aluminated zeolites have higher sorption energy for the xylene of prolate molecular shape—the *p*-xylene molecule. The wide-channel zeolite, BEA, has the strong sorption only for *p*-xylene; for the other isomers, the sorption is weak—in the former case (para), the methyl groups can come in a closer contact with walls of the channels, optimal from the point of view of the dispersion interactions. The o- and m-isomer molecules locate with the aromatic ring plane along the channel axis, and even in such an orientation, the protruding methyl groups cannot get closer to the channel walls. For other zeolites, the sorption is also the strongest for *p*-xylene compared to that for *m*- and *o*-xylene, although the differences are less pronounced. It seems, therefore, that the confinement effect is more decisive than the difference in xylene isomer basicity.

Generally, the introduction of Al in the zeolite structure strengthens sorption; only for *m*-xylene in BEA, it is weaker but only by 7 kcal/mol and is also weaker for *o*-xylene in MFI by 7 kcal/mol. Sorption of *p*-xylene is the strongest for all zeolites, while *o*- and *m*-xylenes yield values more differentiated than in the case of silicalites.

Considering two isomerization mechanisms, the intra- or intermolecular, the former is possible in all studied zeolites, while for the latter, the pore size has the dominant impact. The intermolecular mechanism of xylene isomerization is favored in the large-pore MOR and BEA zeolites. The formation of dicyclic aromatic intermediates was postulated for *m*-xylene isomerization.[14,16] It was found that the reaction can be realized according to the intermolecular mechanism in medium-pore zeolites (with 10-ring channels), if they contain large internal cavities (FAU) or channel intersections (TNU-9, BEA) and in large-pore aluminosilicates (MCM-41). Taking into account that the CHA structure was chosen only as an epitome of the structure with a strong confinement effect, MFI is the zeolite which stabilizes the intermediates C5o (and C7-12 for the other reaction pathway) most strongly.

CONCLUSIONS

This work is aimed at providing the spectroscopic and theoretical insight into the intermediates formed according to the hydrocarbon pool mechanism, which is considered as the main path in the alcohol transformation to higher hydrocarbons. Protonation and methyl-shift processes are deeply investigated in this work since the intermediates related to aromatic ring contraction and its expansion are widely proposed in the literature.

The experimental and computed spectra were compared, and a very good agreement was found in the wavenumbers of the diagnostic bands. The influence of the host on the electronic structure of xylene molecules was confirmed computationally. The presence of the diagnostic 1485 cm^{-1} band was also found for the intermediate structures (protonated 5- and 7-membered ring cations stemming from xylenes). The IR and computational study equivocally showed that the intermediates are more stable in zeolites with narrower channels. Accuracy of the calculation was sufficient to attribute the experimentally observed diagnostic bands. The wavenumbers are reproduced with high accuracy, without scaling. The intensities, however, are not always well reproduced due to the approximation used: the change in the dipole moment, calculated within the Hirshfeld population analysis, upon atomic displacement, used for the calculation of the dipolar transition moment.

In addition to the IR spectra, the adsorption energy of xylenes on silicalite and aluminated zeolites was also obtained. It was found that the protonated forms of xylenes (5- and 7-membered ring) are stabilized in zeolites.

The information concerning the structure of an intermediate in the intramolecular mechanism can be summarized in two branches: the experimental—an intermediate of xylene isomerization exhibits the IR band at 1485 cm^{-1}, regardless of the zeolite structure, and the DFT-based—the total of 18 possible structures of protonated xylenes embedded in four zeolites were modeled (ca. 70 systems). The band close to 1485 cm^{-1} appears in the calculated spectra for 13 out of 16 structures embedded in ZSM-5 zeolite. It was also found that the energy of the intermediate formation depends on the zeolite deprotonation energy, ΔE_{dp}, the stability of the intermediate itself, ΔE_{pr}, and the energy of the zeolite−intermediate interaction, ΔE_{int}.

Based on the spectroscopic results corroborated by the quantum chemical calculations, the following candidates for the intermediates can be postulated (Table 8):

Table 8. Candidates for the Intermediates in the Xylene Isomerization Reactions in MFI, MOR, CHA, and BEA Zeolites[a]

	MFI		MOR		CHA		BEA	
	$\tilde{\nu}_{match}$	E_{stab}	$\tilde{\nu}_{match}$	E_{stab}	$\tilde{\nu}_{match}$	E_{stab}	$\tilde{\nu}_{match}$	E_{stab}
C5o	y	s	y	u	y	s	y	s
C7-12	y	s	n	u	y	u	n	u

[a] $\tilde{\nu}_{match}$—wavenumber matching (yes/no). E_{stab}—stabilization energy: negative (stable, "s") or close to zero ("u").

Note that the y/n flags in the $\tilde{\nu}_{match}$ column mean that the difference between the experimental wavenumber and the simulated one was found not to be exceeding 10 cm^{-1}.

The stability of the C5o intermediate in the small-pore zeolites changes in the following relationship: CHA ≃ MFI > BEA ≃ MOR; the same order is preserved for the concentration of the intermediates.

It can hence be concluded that the OH group acid strength is not a determining factor for the reactivity toward xylene isomerization. More emphasis should be placed on the availability of the OH groups to the diffusing *o*-xylene molecule (readiness for the formation of the transition structure), the energetics of the intermediate product, and the interaction of the *o*-xylene and transition structure with the host framework.

The xylenium ions (the 1485 cm^{-1} band) can therefore be considered as the intermediate species both in the xylene isomerization and ETH process. The formation of protonated xylenes of the respective type and their further transformation through the intra- or intermolecular mechanism are ruled by the size of the internal voids of the zeolite structure. Consequently, the identification of the intermediate products allows us to refer them the respective mechanisms and enables the design of a catalyst for the ETH process characterized by a high selectivity to *p*-xylene.

https://doi.org/10.1021/acs.jpcc.1c01307
J. Phys. Chem. C 2021, 125, 10334−10348

To briefly recapitulate the article, the following main highlights are summarized here:

- The availability of the OH groups allowing for the *o*-xylene molecules to form the TS seems more important for the reactivity in the xylene isomerization than the OH acid strength.
- The other crucial factors are the energetics of the intermediates and the energetics of the *o*-xylene (and the formed transition structures) with the zeolite framework. Indeed, the smaller the cavity formed by intersecting channels (BEA, MOR, and MFI) or cages (CHA), the higher the intensity of the 1485 cm^{-1} band detected in the IR spectra.

AUTHOR INFORMATION

Corresponding Author

Witold Piskorz − *Faculty of Chemistry, Jagiellonian University in Kraków, 30-387 Kraków, Poland;* orcid.org/0000-0002-3462-436X; Email: wpiskorz@chemia.uj.edu.pl

Authors

Gabriela Jajko − *Faculty of Chemistry, Jagiellonian University in Kraków, 30-387 Kraków, Poland;* orcid.org/0000-0001-8286-917X

Karolina Tarach − *Faculty of Chemistry, Jagiellonian University in Kraków, 30-387 Kraków, Poland;* orcid.org/0000-0003-0133-4363

Kinga Góra-Marek − *Faculty of Chemistry, Jagiellonian University in Kraków, 30-387 Kraków, Poland;* orcid.org/0000-0002-1296-9244

Paweł Kozyra − *Faculty of Chemistry, Jagiellonian University in Kraków, 30-387 Kraków, Poland;* orcid.org/0000-0002-7168-5022

Complete contact information is available at: https://pubs.acs.org/10.1021/acs.jpcc.1c01307

Notes

The authors declare no competing financial interest.

ACKNOWLEDGMENTS

The present study was funded by the National Science Centre of Poland (grant 2016/23/B/ST4/00088). Some of the calculations were performed in the Cyfronet PL-Grid supercomputer center in Kraków, Poland. This work was partially financed by the National Science Centre of Poland (grant 2020/37/B/ST4/01215).

REFERENCES

(1) *Zeolites in Industrial Separation and Catalysis*; Kulprathipanja, S., Ed.; Wiley-VCH Verlag GmbH, 2010.

(2) Guisnet, M.; Gilson, J.-P. *Zeolites for Cleaner Technologies*; Catalytic Science Series; Imperial Ccollege Press, 2002; Vol. 3.

(3) Chen, N. Y.; Degnan, T. F.; Smith, C. M. *Molecular Transport and Reaction in Zeolites: Design and Application of Shape Selective Catalysis*; Springer, 1994.

(4) Henriques, C. A.; Monteiro, J. L. F.; Magnoux, P.; Guisnet, M. Characterization of the Coke Formed Duringo-Xylene Isomerization over Mordenites at Various Temperatures. *J. Catal.* **1997**, *172*, 436−445.

(5) Li, Y.-G.; Jun, H. Kinetics study of the isomerization of xylene on ZSM-5 zeolites: the effect of the modification with MgO and CaO. *Appl. Catal., A* **1996**, *142*, 123−137.

(6) Llopis, F.; Sastre, G.; Corma, A. Isomerization and disproportionation of m-xylene in a zeolite with 9- and 10-membered ring pores: Molecular dynamics and catalytic studies. *J. Catal.* **2006**, *242*, 195−206.

(7) Belhekar, A. A.; Ahedi, R. K.; Kuriyavar, S.; Shevade, S. S.; Rao, B. S.; Anand, R.; Tvaruzkova, Z. Effect of acid sites of Al- and Fe-Ferrierite on m-xylene isomerization. *Catal. Commun.* **2003**, *4*, 295−302.

(8) Pérez-Pariente, J.; Sastre, E.; Fornés, V.; Martens, J. A.; Jacobs, P. A.; Corma, A. Isomerization and disproportionation of m-xylene over zeolite *β*. *Appl. Catal.* **1991**, *69*, 125−137.

(9) Corma, A.; Sastre, E. Evidence for a bimolecular isomerization of xylenes on some large pore zeolites. *J. Chem. Soc., Chem. Commun.* **1991**, 594−596.

(10) Zheng, S.; Jentys, A.; Lercher, J. Xylene isomerization with surface-modified HZSM-5 zeolite catalysts: An in situ IR study. *J. Catal.* **2006**, *241*, 304−311.

(11) Mirth, G.; Lercher, J. A. In Situ IR spectroscopic study of the surface species during methylation of toluene over HZSM-5. *J. Catal.* **1991**, *132*, 244−252.

(12) Mirth, G.; Cejka, J.; Lercher, J. A. Transport and isomerization of xylenes over HZSM-5 zeolites. *J. Catal.* **1993**, *139*, 24−33.

(13) Mirth, G.; Lercher, J. A. On the Role of Product Isomerization for Shape Selective Toluene Methylation over HZSM5. *J. Catal.* **1994**, *147*, 199−206.

(14) Min, H.-K.; Cha, S. H.; Hong, S. B. Mechanistic insights into the zeolite-catalyzed isomerization and disproportionation of m-xylene. *ACS Catal.* **2012**, *2*, 971−981.

(15) Gołąbek, K.; Tarach, K. A.; Góra-Marek, K. Standard and rapid scan infrared spectroscopic studies of o-xylene transformations in terms of pore arrangement of 10-ring zeolites − 2D COS analysis. *Dalton Trans.* **2017**, *46*, 9934−9950.

(16) Gołąbek, K.; Tarach, K. A.; Góra-Marek, K. 2D COS analysis of m-xylene transformation over medium-pore zeolites. *Microporous Mesoporous Mater.* **2018**, *266*, 90−101.

(17) Gołąbek, K.; Tarach, K. A.; Filek, U.; Góra-Marek, K. Ethylene formation by dehydration of ethanol over medium pore zeolites. *Spectrochim. Acta, Part A* **2018**, *192*, 464−472.

(18) Gołąbek, K.; Tarach, K. A.; Góra-Marek, K. Xylenes transformation over zeolites ZSM-5 ruled by acidic properties. *Spectrochim. Acta, Part A* **2018**, *192*, 361−367.

(19) Goguen, P. W.; Xu, T.; Barich, D. H.; Skloss, T. W.; Song, W.; Wang, Z.; Nicholas, J. B.; Haw, J. F. Pulse-Quench catalytic reactor studies reveal a carbon-pool mechanism in Methanol-to-Gasoline chemistry on zeolite HZSM-5. *J. Am. Chem. Soc.* **1998**, *120*, 2650−2651.

(20) Niu, X.; Wang, K.; Bai, Y.; Du, Y.-e.; Chen, Y.; Dong, M.; Fan, W. Selective formation of para-xylene by methanol aromatization over phosphorous modified ZSM-5 zeolites. *Catalysts* **2020**, *10*, 484.

(21) Olsbye, U.; Svelle, S.; Bjørgen, M.; Beato, P.; Janssens, T. V. W.; Joensen, F.; Bordiga, S.; Lillerud, K. P. Conversion of methanol to hydrocarbons: how zeolite cavity and pore size controls product selectivity. *Angew. Chem., Int. Ed.* **2012**, *51*, 5810−5831.

(22) Derouane, E.; Nagy, J. B.; Dejaifve, P.; van Hooff, J. H. C.; Spekman, B. P.; Védrine, J. C.; Naccache, C. Elucidation of the mechanism of conversion of methanol and ethanol to hydrocarbons on a new type of synthetic zeolite. *J. Catal.* **1978**, *53*, 40−55.

(23) Sun, J.; Wang, Y. Recent advances in catalytic conversion of ethanol to chemicals. *ACS Catal.* **2014**, *4*, 1078−1090.

(24) van der Borght, K.; Batchu, R.; Galvita, V. V.; Alexopoulos, K.; Reyniers, M.-F.; Thybaut, J. W.; Marin, G. B. Insights into the reaction mechanism of ethanol conversion into hydrocarbons on H-ZSM-5. *Angew. Chem., Int. Ed.* **2016**, *55*, 12817−12821.

(25) Johansson, R.; Hruby, S. L.; Rass-Hansen, J.; Christensen, C. H. The hydrocarbon pool in ethanol-to-gasoline over HZSM-5 catalysts. *Catal. Lett.* **2009**, *127*, 1−6.

(26) Kolboe, S. On the mechanism of hydrocarbon formation from methanol over protonated zeolites. *Stud. Surf. Sci. Catal.* **1988**, *36*, 189−193.

(27) Dahl, I. M.; Kolboe, S. On the reaction mechanism for propene formation in the MTO reaction over SAPO-34. *Catal. Lett.* **1993**, *20*, 329−336.
(28) Dahl, I. M.; Kolboe, S. On the reaction mechanism for hydrocarbon formation from methanol over SAPO-34: 1. Isotopic labeling studies of the Co-reaction of ethene and methanol. *J. Catal.* **1994**, *149*, 458−464.
(29) Dahl, I. M.; Kolboe, S. On the reaction mechanism for hydrocarbon formation from methanol over SAPO-34: 2. Isotopic labeling studies of the Co-reaction of propene and methanol. *J. Catal.* **1996**, *161*, 304−309.
(30) Costa, E.; Uguina, A.; Aguado, J.; Hernandez, P. J. Ethanol to gasoline process: effect of variables, mechanism, and kinetics. *Ind. Eng. Chem. Proc. Des. Dev.* **1985**, *24*, 239−244.
(31) Talukdar, A. K.; Bhattacharyya, K. G.; Sivasanker, S. HZSM-5 catalysed conversion of aqueous ethanol to hydrocarbons. *Appl. Catal., A* **1997**, *148*, 357−371.
(32) Schulz, J.; Bandermann, F. Conversion of ethanol over zeolite H-ZSM-5. *Chem. Eng. Technol.* **1994**, *17*, 179−186.
(33) Svelle, S.; Kolboe, S.; Swang, O.; Olsbye, U. Methylation of alkenes and methylbenzenes by dimethyl ether or methanol on acidic zeolites. *J. Phys. Chem. B* **2005**, *109*, 12874−12878.
(34) Mole, T.; Whiteside, J. A.; Seddon, D. Aromatic co-catalysis of methanol conversion over zeolite catalysts. *J. Catal.* **1983**, *82*, 261−266.
(35) Mole, T.; Bett, G.; Seddon, D. Conversion of methanol to hydrocarbons over ZSM-5 zeolite: An examination of the role of aromatic hydrocarbons using 13carbon- and deuterium-labeled feeds. *J. Catal.* **1983**, *84*, 435−445.
(36) Noda, I. Generalized two-dimensional correlation method applicable to infrared, Raman, and other types of spectroscopy. *Appl. Spectrosc.* **1993**, *47*, 1329−1336.
(37) Sadowska, K.; Góra-Marek, K.; Datka, J. Hierarchic zeolites studied by IR spectroscopy: Acid properties of zeolite ZSM-5 desilicated with NaOH and NaOH/tetrabutylamine hydroxide. *Vib. Spectrosc.* **2012**, *63*, 418−425.
(38) Datka, J.; Góra-Marek, K. IR studies of the formation of ammonia dimers in zeolites TON. *Catal. Today* **2006**, *114*, 205−210.
(39) Delley, B. From molecules to solids with the DMol3 approach. *J. Chem. Phys.* **2000**, *113*, 7756−7764.
(40) Perdew, J. P.; Burke, K.; Ernzerhof, M. Generalized gradient approximation made simple. *Phys. Rev. Lett.* **1996**, *77*, 3865−3868.
(41) Hammer, B.; Hansen, L. B.; Nørskov, J. K. Improved adsorption energetics within density-functional theory using Perdew-Burke-Ernzerhof functionals. *Phys. Rev. B: Condens. Matter Mater. Phys.* **1999**, *59*, 7413−7421.
(42) Delley, B. Hardness conserving semilocal pseudopotentials. *Phys. Rev. B: Condens. Matter Mater. Phys.* **2002**, *66*, 155125.
(43) Benco, L.; Hafner, J.; Hutschka, F.; Toulhoat, H. Physisorption and chemisorption of some n-hydrocarbons at the Brønsted acid site in zeolites 12-membered ring main channels: ab initio study of the gmelinite structure. *J. Phys. Chem. B* **2003**, *107*, 9756−9762.
(44) Göltl, F.; Hafner, J. Modelling the adsorption of short alkanes in protonated chabazite: The impact of dispersion forces and temperature. *Microporous Mesoporous Mater.* **2013**, *166*, 176−184.
(45) Tkatchenko, A.; Scheffler, M. Accurate molecular van der Waals interactions from ground-state electron density and free-atom reference data. *Phys. Rev. Lett.* **2009**, *102*, 073005.
(46) Murnaghan, F. D. The compressibility of media under extreme pressures. *Proc. Natl. Acad. Sci. U.S.A.* **1944**, *30*, 244−247.
(47) Fischer, T. H.; Almlof, J. General methods for geometry and wave function optimization. *J. Phys. Chem.* **1992**, *96*, 9768−9774.
(48) Fletcher, R. *Practical Methods of Optimization*, 2nd ed.; Springer: New York, N.Y., 1980; Vol. *1*: unconstrained optimization.
(49) Halgren, T. A.; Lipscomb, W. N. The synchronous-transit method for determining reaction pathways and locating molecular transition states. *Chem. Phys. Lett.* **1977**, *49*, 225−232.
(50) Broyden, C. G. The convergence of a class of double-rank minimization algorithms 1. General considerations. *IMA J. Appl. Math.* **1970**, *6*, 76−90.
(51) Hirshfeld, F. L. Bonded-atom fragments for describing molecular charge densities. *Theor. Chim.* **1977**, *44*, 129−138.
(52) Mayer, I. Charge, bond order and valence in the ab initio SCF theory. *Chem. Phys. Lett.* **1983**, *97*, 270−274.
(53) Sazama, P.; Tabor, E.; Klein, P.; Wichterlova, B.; Sklenak, S.; Mokrzycki, L.; Pashkkova, V.; Ogura, M.; Dedecek, J. Al-rich beta zeolites. Distribution of Al atoms in the framework and related protonic and metal-ion species. *J. Catal. Catalysis* **2016**, *333*, 102−114.
(54) van Bokhoven, J. A.; Lamberti, C. Structure of aluminum, iron, and other heteroatoms in zeolites by X-ray absorption spectroscopy. *Coord. Chem. Rev.* **2014**, *277*−*278*, 275−290.
(55) Olson, D. H.; Khosrovani, N.; Peters, A. W.; Toby, B. H. Crystal structure of dehydrated CsZSM-5 (5.8Al): Evidence for nonrandom aluminum distribution. *J. Phys. Chem. B* **2000**, *104*, 4844−4848.
(56) Akporiaye, D. E.; Dahl, I. M.; Mostad, H. B.; Wendelbo, R. Aluminum distribution in chabazite: An experimental and computational study. *J. Phys. Chem.* **1996**, *100*, 4148−4153.
(57) Oumi, Y.; Kanai, T.; Lu, B.; Sano, T. Structural and physicochemical properties of high-silica mordenite. *Microporous Mesoporous Mater.* **2007**, *101*, 127−133.
(58) Karcz, R.; Dedecek, J.; Supronowicz, B.; Thomas, H. M.; Klein, P.; Tabor, E.; Sazama, P.; Pashkova, V.; Sklenak, S. TNU-9 zeolite: aluminum distribution and extra-framework sites of divalent cations. *Chem.—Eur. J.* **2017**, *23*, 8857−8870.
(59) Pine, L.; Maher, P. J.; Wachter, W. A. Prediction of cracking catalyst behavior by a zeolite unit cell size model. *J. Catal.* **1984**, *85*, 466−476.
(60) Al-Khattaf, S.; Ali, S. A.; Aitani, A. M.; Žilková, N.; Kubička, D.; Čejka, J. Recent advances in reactions of alkylbenzenes over novel zeolites: the effects of zeolite structure and morphology. *Catal. Rev.* **2014**, *56*, 333−402.
(61) Boronat, M.; Corma, A. What is measured when measuring acidity in zeolites with probe molecules? *ACS Catal.* **2019**, *9*, 1539−1548.
(62) Derouane, E.; Andre, J.-M.; Lucas, A. A. Surface curvature effects in physisorption and catalysis by microporous solids and molecular sieves. *J. Catal.* **1988**, *110*, 58−73.
(63) Derouane, E. G. Zeolites as solid solvents. *J. Mol. Catal. A: Chem.* **1998**, *134*, 29−45.
(64) Deshlahra, P.; Iglesia, E. Reactivity descriptors in acid catalysis: acid strength, proton affinity and host−guest interactions. *Chem. Commun.* **2020**, *56*, 7371−7398.
(65) Mangold, M.; Rolland, L.; Costanzo, F.; Sprik, M.; Sulpizi, M.; Blumberger, J. Absolute pK a values and solvation structure of amino acids from density functional based molecular dynamics simulation. *J. Chem. Theory Comput.* **2011**, *7*, 1951−1961.
(66) Lee, C.; Parrillo, D. J.; Gorte, R. J.; Farneth, W. E. Relationship between differential heats of adsorption and Brønsted acid strengths of acidic zeolites: H-ZSM-5 and H-Mordenite. *J. Am. Chem. Soc.* **1996**, *118*, 3262−3268.
(67) Parrillo, D. J.; Lee, C.; Gorte, R. J. Heats of adsorption for ammonia and pyridine in H-ZSM-5: evidence for identical Brønsted-acid sites. *Appl. Catal., A* **1994**, *110*, 67−74.
(68) Tsutsumi, K.; Nishimiya, K. Differential molar heats of adsorption of ammonia on silicious mordenites at high temperature. *Thermochim. Acta* **1989**, *143*, 299−309.
(69) Suzuki, K.; Sastre, G.; Katada, N.; Niwa, M. Periodic DFT calculation of the energy of ammonia adsorption on zeolite Brønsted acid sites to support the ammonia IRMS−TPD Experiment. *Chem. Lett.* **2009**, *38*, 354−355.
(70) Nachtigallová, D.; Bludský, O.; Otero Areán, C.; Bulánek, R.; Nachtigall, P. The vibrational dynamics of carbon monoxide in a confined space - CO in zeolites. *Phys. Chem. Chem. Phys.* **2006**, *8*, 4849−4852.

https://doi.org/10.1021/acs.jpcc.1c01307
J. Phys. Chem. C 2021, 125, 10334−10348

(71) Gutsev, G. L.; Boldyrev, A. I. DVM-Xα calculations on the ionization potentials of complex anions and the electron affinities of MXk_{+1} "superhalogens". *Chem. Phys.* **1981**, *56*, 277−283.
(72) Czapla, M.; Skurski, P. Toward the preparation of the $HAuF_6$, HAu_2F_{11}, and HAu_3F_{16} superacids: Theoretical study. *Int. J. Quantum Chem.* **2018**, *118*, No. e25494.

https://doi.org/10.1021/acs.jpcc.1c01307
J. Phys. Chem. C 2021, 125, 10334−10348